heritage

MDPI

Article

Microanalytical Investigation of Prehistoric Colorants from Uralian Rock Art (Ignatievskaya Cave and Idrisovskaya II and Zmiev Kamen' Pictographs)

Daria Kiseleva [1,*], Evgeny Shagalov [1,2], Elizaveta Pankrushina [1], Vladimir Shirokov [3], Arina Khorkova [1,4] and Danil Danilov [4]

[1] A.N. Zavaritsky Institute of Geology and Geochemistry, Ural Branch of Russian Academy of Sciences, 15 Akademika Vonsovskogo str., 620110 Ekaterinburg, Russia
[2] Department of Mineralogy, Petrography, and Geochemistry, Ural State Mining University, 30 Kuybysheva Str., 620014 Ekaterinburg, Russia
[3] Institute of History and Archaeology, Ural Branch of Russian Academy of Sciences, 16 Sofyii Kovalevskoy Str., 620108 Ekaterinburg, Russia
[4] Institute of Physics and Technology, Ural Federal University named after the first President of Russia B. N. Yeltsin, 21 Mira Str., 620002 Ekaterinburg, Russia
* Correspondence: kiseleva@igg.uran.ru

Abstract: Uralian parietal and rock art (cave paintings and pictographs, or "pisanitsy") represents a unique archaeological and cultural phenomenon, comprising 90 sites stretching for more than 800 km from north to south, which date from the Paleolithic era extending into the present Holocene epoch. The identification of the nature of prehistoric colorants provides an insight into their provenance, manufacture and utilization, as well as contributing to the conservation and restoration of drawings. The studies of mineral, elemental and organic phase composition of the colorant micro-samples from the drawings of Ignatievskaya cave and Idrisovskaya II and Zmiev Kamen' pictographs (Southern and Middle Urals, Russia) discussed in the present work were carried out using a special set of microspectroscopic methods (SEM-EDS and Raman spectroscopy) offering high spatial resolution. The fatty acid composition of the organic phase was analyzed by GC–MS. The technology of colorant manufacture could have included thorough grinding and mixing of unheated hematite with an organic binder made from animal fat and a clayey extender in order to achieve the desired hue and intensity of the color. It is possible that the colorant was applied in layers (Idrisovskaya II and Zmiev Kamen' pictographs). The development of authigenic phosphate and sulfate (gypsum) mineralization, which is observed in all studied sites, as well as oxalate encrustation on the Idrisovskaya II pictograph, indicates the conditions and processes of secondary mineral formation.

Keywords: parietal art; prehistoric Uralian pictographs; Ignatievskaya cave; Idrisovskaya II and Zmiev Kamen' pictographs; mineral pigments; Raman spectroscopy; hematite; organic binder; fatty acids; rock art

Citation: Kiseleva, D.; Shagalov, E.; Pankrushina, E.; Shirokov, V.; Khorkova, A.; Danilov, D. Microanalytical Investigation of Prehistoric Colorants from Uralian Rock Art (Ignatievskaya Cave and Idrisovskaya II and Zmiev Kamen' Pictographs). *Heritage* **2023**, *6*, 67–89. https://doi.org/10.3390/heritage6010004

Academic Editor: Vittoria Guglielmi

Received: 21 November 2022
Revised: 16 December 2022
Accepted: 17 December 2022
Published: 21 December 2022

1. Introduction

Parietal art, including cave paintings and rock art, is one of the most widespread and information-rich archaeological artefacts. Such prehistoric drawings covering rock outcrops occur in more than 120 countries of the world across diverse geographical, geomorphological, and climatic environments, from caves and grottos to mountain plateaus, from tundras to deserts [1].

Many ancient and prehistoric Ural pictographs, also called "pisanitsy" or "painted rocks", are located on rock outcrops typically occurring along the banks of rivers (Chusovaya, Tagil, Rezh, Neyva, Ufa, Iset', Irbit, Belaya, Yuruzan' and others) and—less often—lakes, covering a total area extending from north to south for about 800 km [1].

Current ideas about the dating of Ural parietal art works are mainly based on analogies with dated archaeological items and rock figures obtained from other regions; radiocarbon datings have so far been obtained only for the paintings from the Ignatievskaya cave. However, by carefully cross-analyzing figurative and non-figurative motifs, it is possible to determine the time of creation of the Ural pictographs as having mainly occurred during the Eneolithic and Bronze Ages [1].

At present, more than 90 sites with prehistoric parietal art have been discovered in the Urals, with two main localization areas: on the eastern slope of the Middle Urals along the rivers Tagil (20 pictographs), Neiva and Rezh; and on the western Southern Urals slope along the rivers Ai and Yuryuzan [1].

Pictographic art has been applied to various rocks characteristic of one or another part of the Urals; thus, the river banks of the western slope are predominantly composed of limestone, while on the eastern slope granites, syenites, gabbro and diorites prevail along with gneisses and shales [1]. In contrast to the multiple techniques applied for creating images in Siberia or the European North, such as drawing with paint, embossing, engraving, grinding and their combinations, Uralian pictographs (with a few exceptions) present monochromatic drawings [1].

Color is an extremely important aspect of the study of art and archaeological objects. By identifying the nature of the pigments used in archaeological artefacts, we gain an insight into their provenance, manufacture, use, exchange, alterations, as well as solutions to issues occurring due to the changes in pigment colors over time, and hence, problems with their conservation and restoration [2]. From archaeological and historical perspectives, a study of the composition of colorants can reveal the level of technology necessary for their creation, lead to a deeper understanding of the compositional styles and chronology of rock paintings, and form a basis for an identification of the cultural traditions of their creators [3].

The introduction of the physicochemical and geochemical methods and approaches into the studies of cultural heritage objects and archaeological artefacts has found application in the investigation of rock art [2–13]. Recipes of prehistoric paintings frequently include inorganic substances, mainly red-orange, black and white pigments that might have been mixed with organic binders of vegetable or animal origin and extenders in order to achieve the particular hue [1,2,7–16]. Since most natural organic molecules cannot be used as colorants in artworks due to their weathering and fading with light, reactions with other chemicals (oil, resins, substrates, etc.) of the artwork itself or pollutants, the minerals have played a major role in the use of pigments due to higher stability [2]. Natural-colored minerals are known from prehistoric times (red and yellow ochres, black manganese oxides, carbon black). Ferric oxide monohydrate $Fe_2O_3 \cdot H_2O$ or FeOOH (goethite), when mixed with silica and clay, provides a yellow color (yellow ochre), while red ochre, which may be produced by heating the yellow ochre to anhydrous ferric oxide Fe_2O_3 (hematite), may also occur naturally [2,14,15]. The pigments used for obtaining white color are calcite, or white clay or shale [14,15], or beeswax [12]. Manganese oxides and carbon are responsible for black color [2,12,14,15].

One of the imperative challenges when sampling the rock art objects involves maintaining the intactness of the pictograph, ideally using in situ non-destructive techniques as demonstrated for the first time by Tournié et al. [15] for on-site Raman spectroscopic studies of San rock art (South Africa) and now widely applied in studies of rock art (see the reviews by Rusaki and Vandenabeele [17] and Hernanz et al. [4]). If the extraction of samples is justified and unavoidable (dating, GC–MS), these must be minimized so as to take only micro-specimens from areas affected by exfoliation, flaking or spallation areas of the painting panel surface in such a way that the extraction area is negligible to the naked eye [4]. Here, samples must be removed with extreme care to avoid contamination using sterile surgical blades or Dremel micro-tools. Very small granules of pigment (<1 mm^2) may be extracted, together with rock flakes and accretions. In general, their removal should have a minimal effect on the pictographs and their surrounding area.

In parallel to sampling the pictorial areas, samples from their surroundings should also be collected in order to compare the geological setting both with and without the paint layer [4].

Further laboratory investigation of such micro-samples (some millimeters in size and tens of milligrams by weight) involves selecting from a number of microspectroscopic techniques, including those with higher degree of visualization (imaging and mapping): even a single mineral grain can possess great informational potential, whether in terms of morphological features, elemental distributions, or structural irregularities.

Representing a scientifically elegant technique for pigment analysis of archaeological materials, Raman spectroscopy is used in an ever-growing number of research areas in cultural heritage (archaeometry and analysis of artefacts) [2,4]. This is a rapid, non-destructive vibrational spectroscopic technique for studying various mineral and organic species with high spatial resolution (~1 μm), requiring minimal sample preparation and offering the ability to perform Raman imaging and hypermapping operations using hydrated and dehydrated specimens.

The molecular and mineralogical characterization of rock art materials by Raman spectroscopy may be complemented by other microscopic techniques, such as scanning electron microscopy combined with energy-dispersive X-ray spectrometry or electron probe microanalysis with wavelength-dispersive X-ray spectrometry, which provide images (in back-scattered and secondary electron modes) and elemental composition, as well as, using graphical software, elemental maps.

Known and hypothetical organic binding agents in rock art include plant juices or oils, urine, animal fat, bone marrow, blood, eggs (yolk and/or albumen), as well as human saliva [4,18–20]. While organic binding agents are typically contemporaneous with paint production, these materials often degrade over time and become difficult to characterize [18]. Lipids (fats, waxes and resins) can survive for longer periods of time due to their hydrophobic properties, i.e., they are not readily dissolved in water. The need to study the low contents of preserved lipid components in archaeological samples necessitates the development and application of suitable extraction, purification and analysis methods by gas chromatography–mass spectrometry (GC–MS), the method most often used for qualitative and quantitative analysis of complex organic mixtures, including those of archaeological origin [4,6,21–23].

This article develops the microanalytical approach to the studies of colorants from a number of Uralian cave paintings and pictographs (Ignatievskaya cave and Idrisovskaya II and Zmiev Kamen' pictographs), applied earlier to the investigation of prehistoric and experimental (30 years old) drawings from the Dvuglazy Kamen' pictograph (Neyva River, middle Urals [6]. The approach employs the combination of the SEM-EDS analysis of elemental composition and Raman spectroscopic identification of mineral composition and GC–MS determination of the organic compounds (fatty acids) of the microscopic colorant samples.

As well as adding to the existing knowledge of compositions of inorganic mineral pigments and possible extenders added to the colorant mixtures and that of the organic compounds comprising the binder, it is hoped that the reported investigation will serve to refine and critically revise our earlier results obtained from the Ignatievskaya cave [24] and Zmiev Kamen' pictograph [3].

2. Materials and Methods

The elemental, mineral and organic composition of the paintings at three parietal art sites across the Southern and Middle Urals (Russia), along with their corresponding rock panels (substrates), was investigated using microspectroscopic and GC–MS techniques (Figure 1).

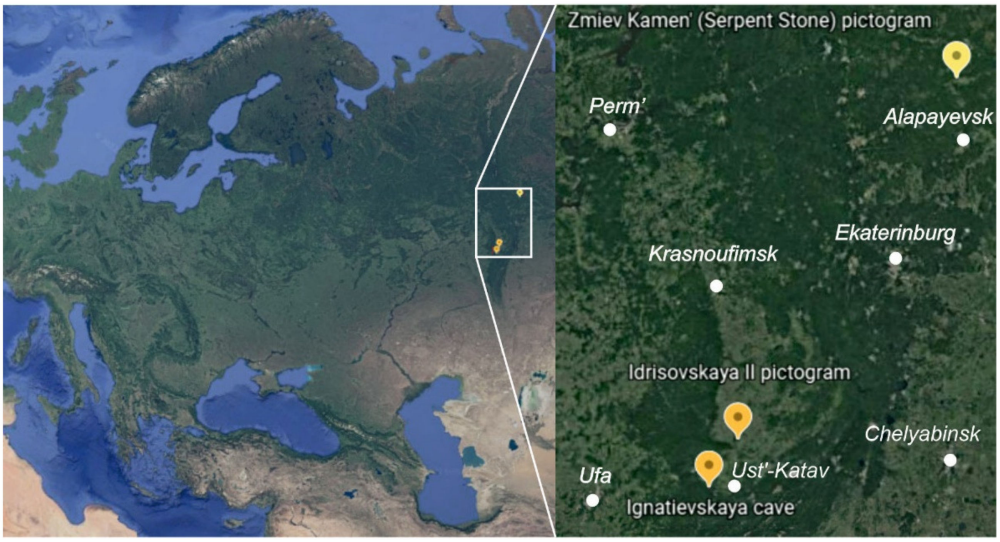

Figure 1. Geographical location of the sites with cave paintings (Ignatievskaya cave) and pictographs (Zmiev Kamen' and Idrisovskaya II).

The Ignatievskaya (Yamazy-Tash) cave is located in the northwestern foothills of the southern Ural Mountains (the Katav-Ivanovsk district of the Chelyabinsk region, Russia), on the right bank of the Sim River, a tributary of the Belaya River. Forming the largest cave in the karst region, it is situated in Devonian limestones. Along with the neighboring Kapova (Shulgan-Tash) cave, it hosts the easternmost occurrences of Paleolithic cave art in Europe. The Ignatievskaya cave became world famous after the discovery of ancient drawings in 1980 by Russian archaeologists V.T. Petrin, S.E. Chairkin and V.N. Shirokov [25,26]. It preserves representational images of a mammoth and a horse, as well as various fantastic and composite animals, anthropomorphic creatures and non-figurative motifs.

Three early conventional ^{14}C datings of charcoal and bones from the cultural layer yielded Upper Paleolithic ages (18.3–15.4 cal ka BP [25]). The chronology was recently refined by accelerator mass spectrometry (AMS) dating of charcoal and bones from the cultural layers associated with artistic activity, with four dates constraining the time of its accumulation to 17.4–16.3 cal ka BP [27]. The dates are consistent with paleontological evidence from the cultural layer, represented by Late Pleistocene fauna [25] and pollen characteristic of uniform, forest-free vegetation of a periglacial steppe [28]. Upper Paleolithic dates are broadly consistent with ^{230}Th dates obtained on flowstone underlying and covering paintings [29]. Although three earlier ^{14}C determinations made directly on the charcoal paintings returned Mesolithic rather than Upper Paleolithic dates (8.9–6.6 cal ka BP [30]), they appeared younger than the flowstone that formed after both red and black paintings were made [29]. At the time of publication, Steelman et al. [30] acknowledged that their dates appear "unexpectedly recent" (p. 347) and offered four explanations of the inconsistency, three of which questioned the presumed Paleolithic antiquity of paintings, while one suggested a conflation of two painting episodes. Later, the images of the Ice Age were also found in the Serpievskaya II (Kolokol'naya) cave, near the Ignatievskaya cave [26,31].

The Idrisovskaya II open-air pictograph is located in the Salavat district of Bashkortostan, Russia, on the left bank of the Yuryuzan river (Figure 1). It is situated in Lower and Middle Carboniferous limestones. The archaeological site at the Idrisovskaya cave is correlated with the early Late Paleolithic [32,33]. Drawings of animals, anthropomorphic creatures and non-figurative motifs are located at the bottom of the rock shelter under the Idrisovskaya cave. Excavations revealed a sacrificial site including bone remains of animals and humans, fragments of ocher and pieces of hematite cut with ancient saws, stone products and the fragments of clay pottery from the Chalcolithic, Bronze and Iron Ages [32].

The Zmiev Kamen' open-air pictograph is located in the granite and amphibolite outcrops on the left bank of the Tagil river near the village of Machnevo (Sverdlovsk region, Russia) (Figure 1). The pictograph is characterized by the numerous drawings combined into 9 groups demonstrating animals, geometric figures and signs, anthropomorphic creatures and non-figurative motifs [1,3,34].

During the sample collection, conservation concerns and ethical considerations were taken into account. To ensure minimal intervention, microscopic fragments (several mm in size, weighing 10–100 mg) were carefully scraped from cracks in the rock or the thickest paint layers using a medical scalpel in order to protect the integrity of drawings. Where possible, two or more samples were taken from different areas of a painting.

Fragments of red and black colorants were analyzed: the Great Hall of the Ignatievskaya cave (red colorant from the panel near the cruciform sign and near a small red horse, black colorant from an arrow-shaped sign, black matter of natural origin from a rock crack); the Idrisovskaya II pictograph (red colorant from the pictograph); the Zmiev Kamen' (red colorant from the pictograph). Along with the colorants, the underlying rock substrate was analyzed in all cases.

Raman spectra and SEM-EDS analyses were obtained in the Geoanalitik shared research facilities of the IGG UB RAS. The re-equipment and comprehensive development of the Geoanalitik shared research facilities of the IGG UB RAS is generously supported by a grant of the Ministry of Science and Higher Education of the Russian Federation (Agreement No. 075-15-2021-680).

For scanning electron microscopic (SEM) studies, the samples were mounted onto conductive carbon adhesive tape and carbon-sputtered. The remaining un-sputtered portions of samples were used for the purposes of Raman microspectroscopic investigation.

SEM images, EDS analyses and elemental maps of samples were obtained using a JEOL JSM-6390LV scanning electron microscope equipped with an INCA Energy 450 X-Max EDS spectrometer and AZtecOne software with an accelerating voltage of 20 kV and an exposure time of 5 ms per pixel.

The mineral phases were identified using a LabRAM HR800 Evolution confocal Raman spectrometer equipped with an Olympus BX-FM optical microscope. An Olympus 50× objective (numerical aperture = 0.7), a diffraction grating of 600 gr/mm and an electrically cooled CCD detector were used for recording. The spectrometer calibration was guided along the Rayleigh line and the emission lines of a neon lamp. The spatial resolution was up to 1 μm. Laser power of about 5–10 mW was applied behind the objective lens for excitation by He-Ne (633 nm) and Ar- (488 nm) gas lasers. Acquisition time was 5–50 s per 10–50 accumulations depending on the degree of fluorescence displayed by the samples. As a result, Raman spectra were obtained in the range of 150–2000 cm^{-1}. In fact, the spectra were recorded covering the range of Rayleigh scattering to control the positions of the vibrational modes. A useful Raman signal was recorded against the background of an extended growing bright photoluminescent signal of a mixed cumulative nature. The resulting superimposed spectra were processed; the low-energy range from ~100–150 cm^{-1} was cut off and the background was subtracted using a linear function. The identification of mineral phases was carried out using the KnowItAll (Bio RAD) database integrated into the spectrometer software and the RRUFF.INFO database.

The chromatographic analyses were performed at a facility hosted by the Ural Federal University. For the determination of fatty acid methyl esters (FAME) by gas chromatography with mass-spectrometric detector, sample weights of 10–100 mg were used. Fatty acids (FAs) were extracted from the weighed samples using a chloroform: methanol (2:1) mixture. To assist their dissolution, they were placed into an ultrasound bath for 20 min. The samples were centrifuged for 10 min at 3000 rpm. The extract obtained was placed into vacuum to remove the solvent. The dry residue was dissolved in acetonitrile and derivatized with dimethylformamide-dimethyl acetal. To perform gas chromatography–mass spectrometry (GC–MS) using a Perkin Elmer Clarus 600T mass spectrometer, the samples were injected into a capillary column in splitless mode

(Elite-5MS 30 m × 250 μm); the thickness of the stationary phase layer was 0.25 μm. The injector temperature was 200 °C with a 1 min evaporation phase. The GC program consisted in a uniform increase in temperature from 30 to 300 °C at a rate of 10 °C/min, followed by an isothermal period at T = 300 °C for 5 min. The total time of the analysis was 32 min. MS was conducted in the mode of electron impact ionization (EI) at a gas chromatographic interface temperature of 200 °C; the cathode temperature was 180 °C, while the ion source voltage was 70 eV. Mass spectra were obtained in the range of the mass-to-charge ratio of 35–400 a.m.u. The peaks were identified using the integral mass spectral library and literature data.

3. Results

3.1. Ignatievskaya Cave

Figure 2 depicts a photograph of the sampled area (red colorant from the red panel near the cruciform sign in the Great Hall of the Ignatievskaya cave) (a), a BSE image of the colorant fragment (b), and the elemental maps of P, Na, Si, Al, Mg, S, Ca, K, Ti, Cl and Fe (c).

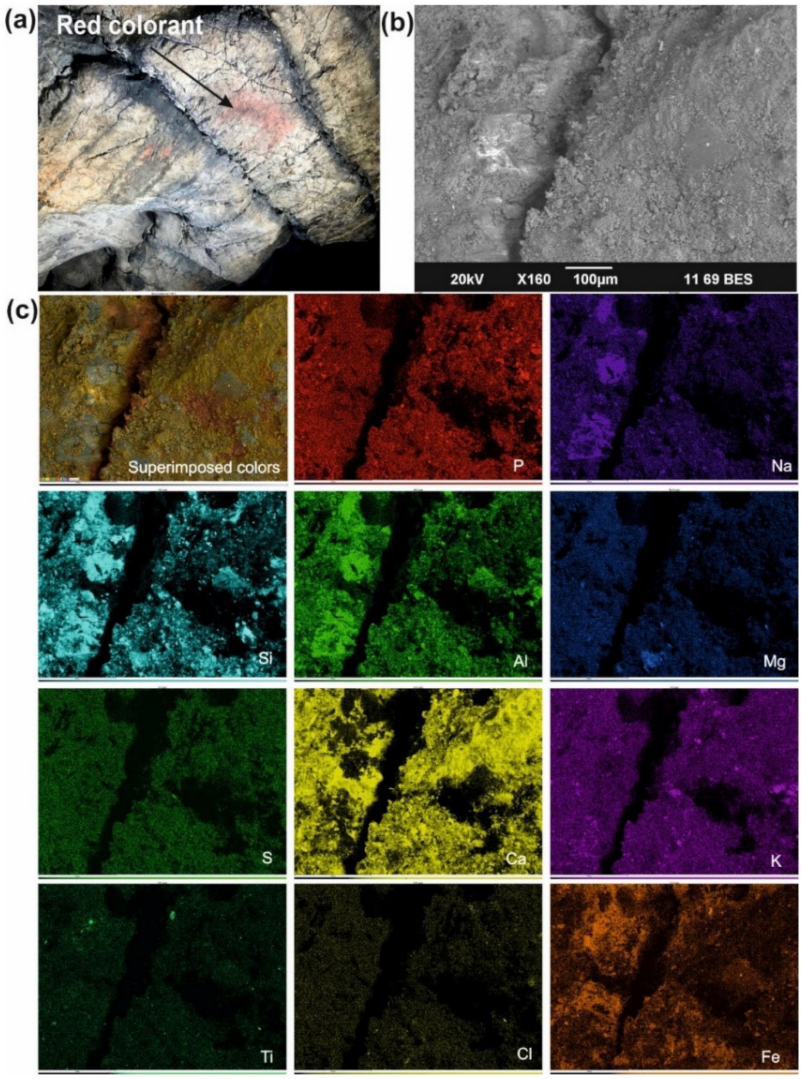

Figure 2. (**a**) Photograph of the sampled area (red colorant from the red panel near the cruciform sign, the Great Hall of the Ignatievskaya cave); (**b**) BSE image of the red colorant fragment; (**c**) the same image in superimposed colors and the elemental maps of P, Na, Si, Al, Mg, S, Ca, K, Ti, Cl and Fe.

Grains (up to 30 μm in size) of quartz, feldspar and calcite from the rock substrate, as well as small grains (<5 μm in size) of hydromicous mineral containing iron and/or a fine admixture of hematite, were found in the red colorant. Traces of phosphorus, sulfur and chlorine are recorded in the spectrum. An apatite grain (100 × 30 μm) was identified. No carbon was recorded in red colorants.

In the black colorant (Figure 3a), crystals of magnesium-containing calcite with a fine coating of carbon were found. Well-formed gypsum crystals with a size of 100–200 μm were visible in BSE images (Figure 3b,c) along with the thin coating of hydromicous material and traces of iron and phosphorus (Figure 3d). The black substance of natural origin from the rock cracks (which could be easily confused with artificial drawing) was characterized by the presence of small (10–50 μm) calcite and quartz grains (Figure 4d), along with rare grains of accessory minerals such as ilmenite and zircon, which were distributed among the fine hydromicous mineral with traces of phosphorus and sulfur. The presence of accessory minerals could be associated with the supergene geological setting including nearby iron ore and iron–titanium deposits.

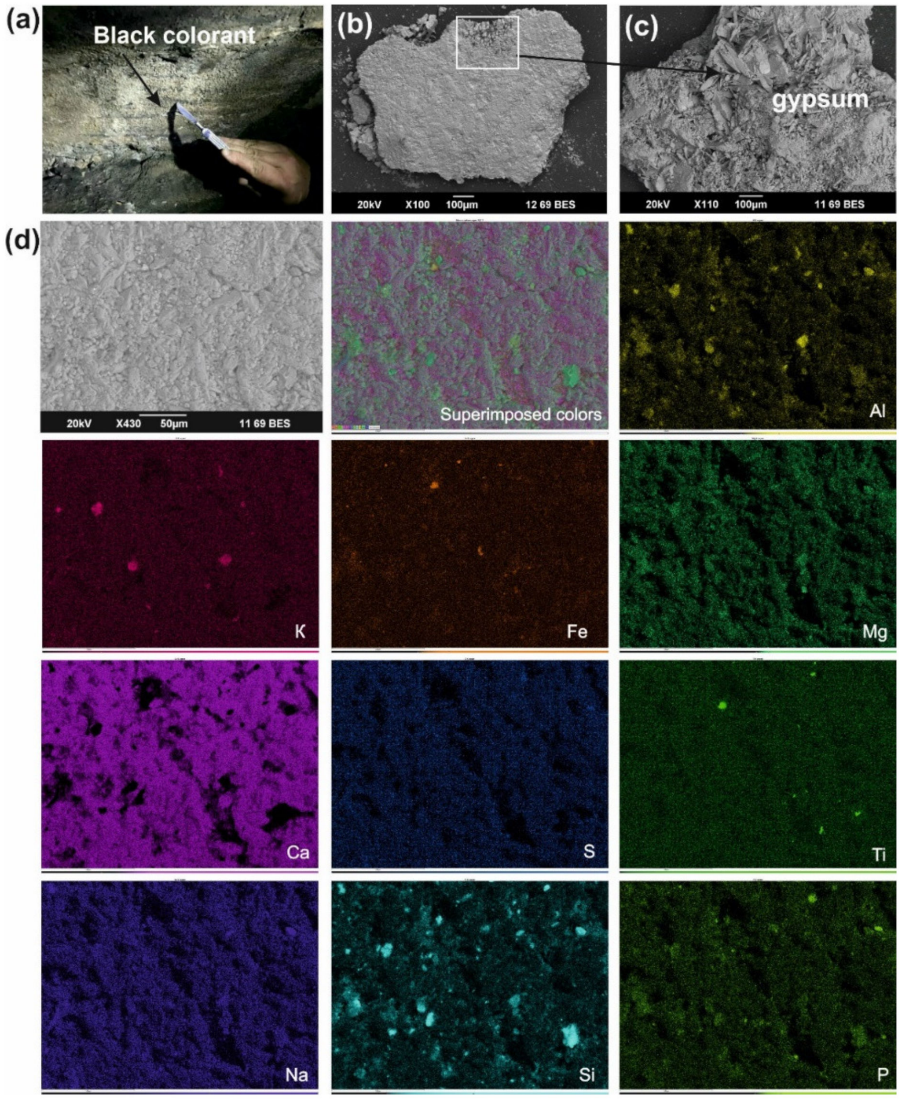

Figure 3. (**a**) Photograph of the sampled area (black colorant from an arrow-shaped sign, the Great Hall of the Ignatievskaya cave); (**b**) BSE image of the colorant fragment; (**c**) Gypsum crystals at higher magnification; (**d**) BSE image, the same image in superimposed colors and the elemental maps of P, Na, Si, Al, Mg, S, Ca, K, Ti and Fe.

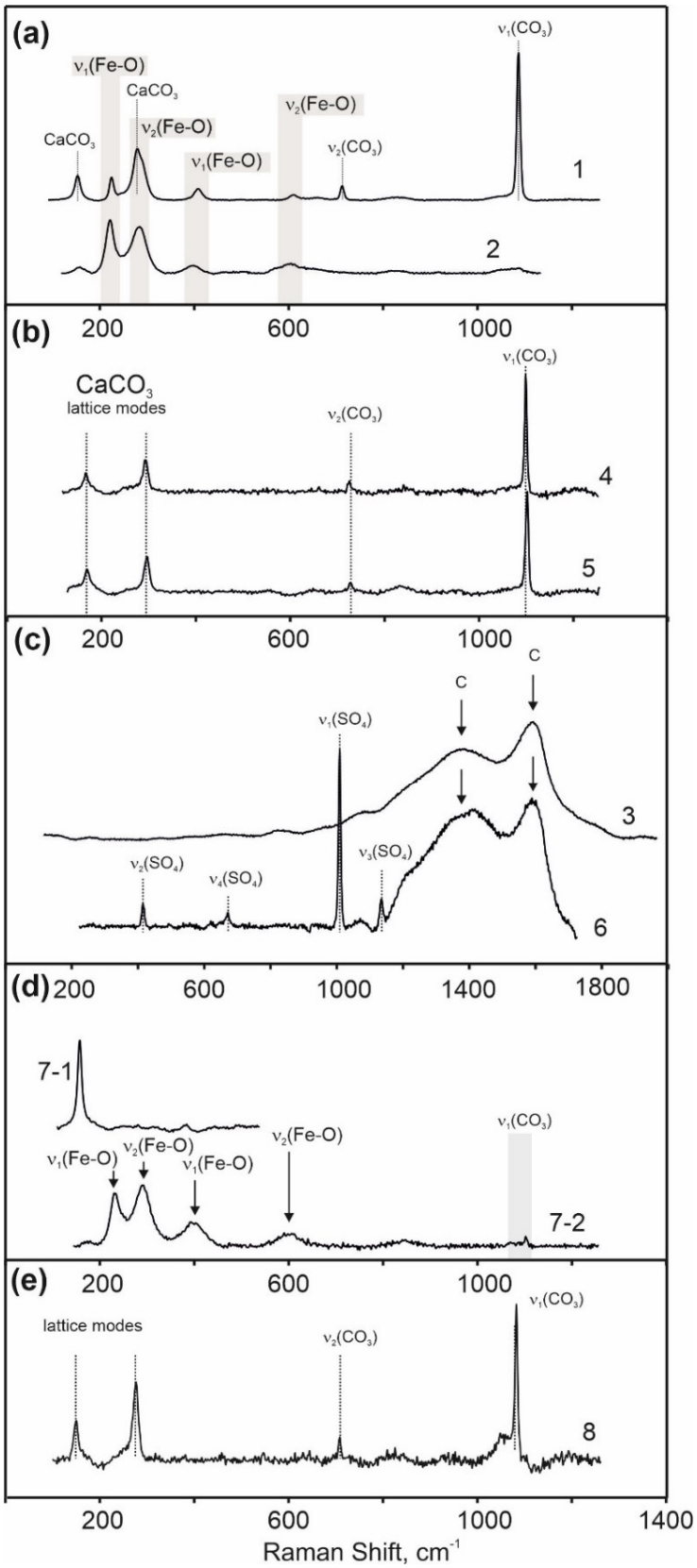

Figure 4. Raman spectra of the colorants from the Great Hall of the Ignatievskaya cave: (**a**) 1—red colorant and 2—hematite from the excavations of the Idrisovskaya cave demonstrated for comparison; (**b**) 4—mondmilch (moon milk) and 5—newly formed calcite; (**c**) 3 and 6—black colorant from an arrow-shaped sign; (**d**) 7–1 and 7–2—black substance of natural origin from rock cracks; (**e**) 8—calcite from stalagmite.

The presence of hematite in red pigment is confirmed by Raman microspectroscopy (Figure 4a).

The presence of carbon black in the black colorant was confirmed by Raman microspectroscopy (Figure 4c). For comparison, a number of newly formed minerals such as mondmilch (moon milk), calcite and a fragment of stalagmite were analyzed by Raman spectroscopy (Figure 4b,e).

3.2. Idrisovskaya II Pictograph

In the rock panel of the Idrisovskaya II pictograph (Figure 5a), fine-grained crystals of calcite (Figure 5c,d) and dolomite with traces of weathering (leaching) were found along the cleavage (Figure 6) together with gypsum crystals.

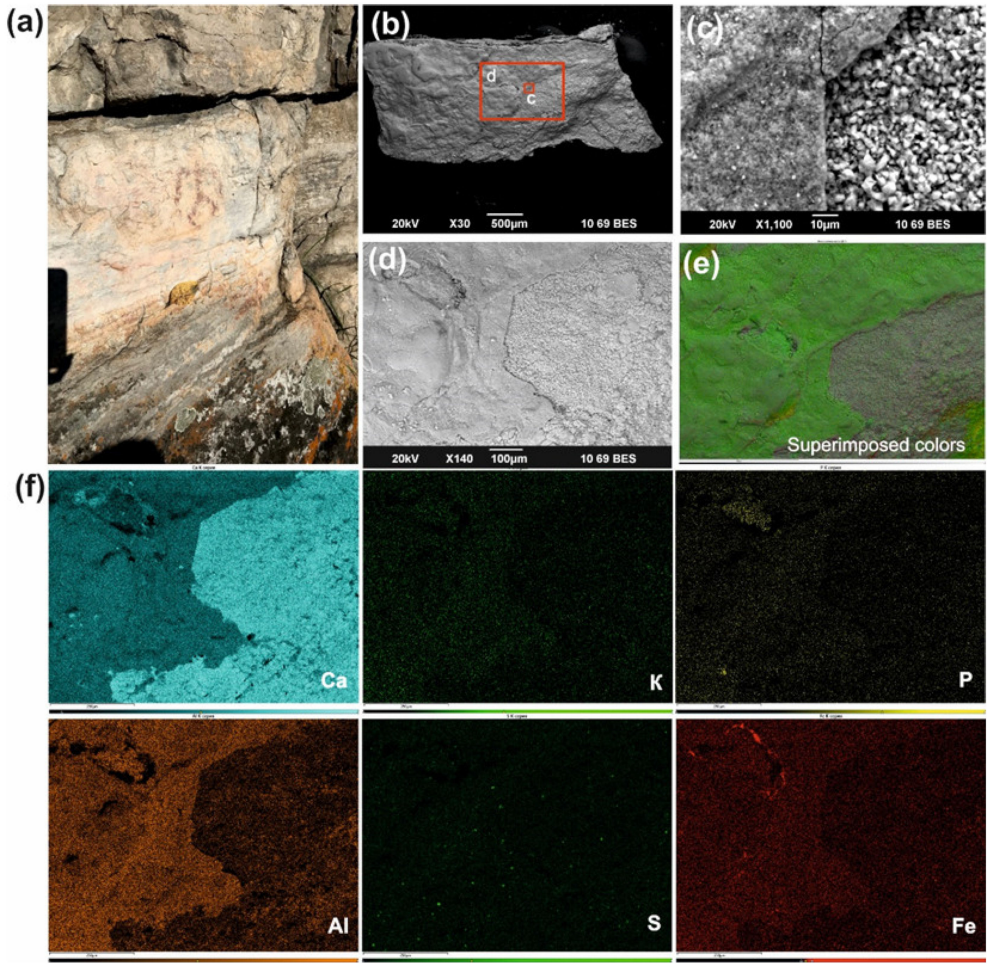

Figure 5. (**a**) Photograph of the sampled area from the Idrisovskaya II pictograph; (**b**) BSE image of the red colorant fragment; (**c**) magnified c site; (**d**) magnified d site; (**e**) image of d area in superimposed colors; (**f**) elemental maps of P, Al, S, Ca, K and Fe.

The colorant layer with a thickness of about 10–20 µm consisted of several layers (possible traces of renewal) (Figure 5a,d,e). The very finely powdered (<1–5 µm) material of colorant consisted of siliceous, hydromicaceous and ferrous compounds (hematite, as identified by Raman spectroscopy, Figure 7b) with the admixture of phosphorus and sulfur.

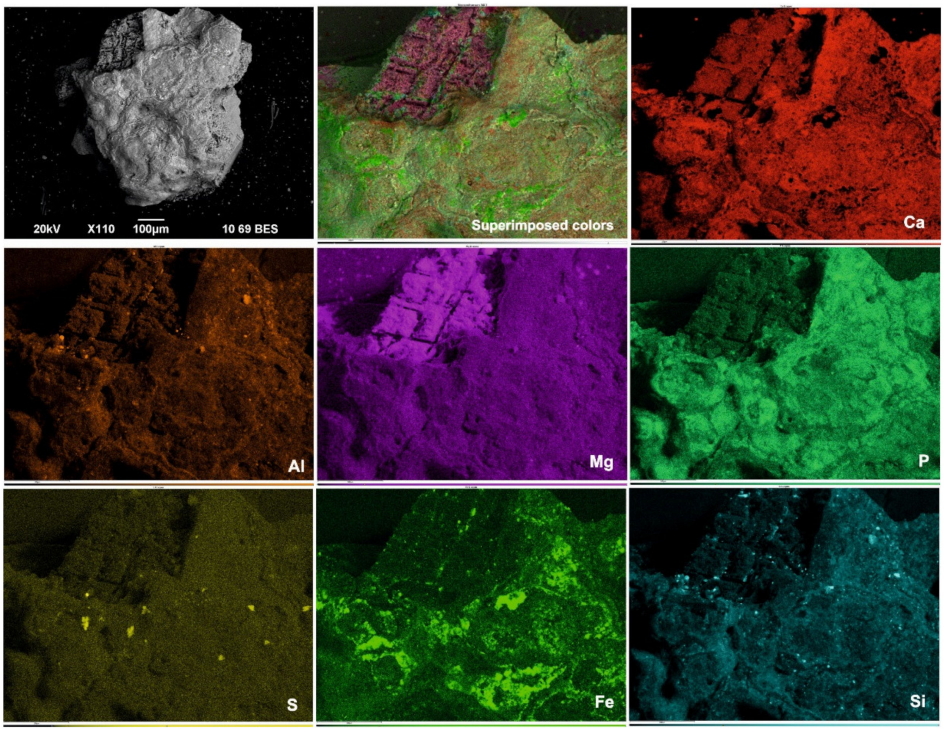

Figure 6. BSE image of the red colorant fragment from the Idrisovskaya II pictograph and its magnified area in superimposed colors with the elemental maps of P, Al, Mg, S, Ca, Si and Fe.

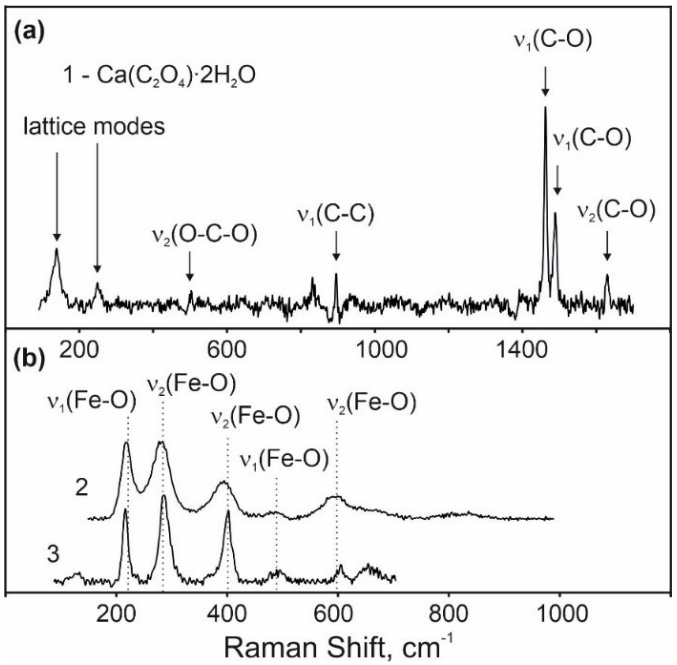

Figure 7. Raman spectra of the red colorant from the Idrisovskaya II pictograph: (**a**) 1—whewellite filling the micro-cracks on the surface of red colorant; (**b**) 2—red colorant and 3—hematite from the excavations of the Idrisovskaya cave.

Since the particles of hematite were practically indistinguishable in the colorant, its presence could be judged only by the data of elemental and Raman analysis (Figures 5f and 7b).

The whitish substance filling the micro-cracks on the surface of red colorant was identified as whewellite (calcium oxalate) by Raman spectroscopy (Figure 7a).

3.3. Zmiev Kamen' (Serpent Stone) Pictograph

In order to estimate the thickness of colorant layer, a cleavage perpendicular to the colored surface was studied by SEM-EDS (Figure 8a). The colorant layer, having a thickness of around 30 µm, was situated on top of a layered structure (Figure 8b). The rock panel was composed mostly of granite and amphibolites (Figure 8f). A large amount of calcium sulfates(brighter areas in Figure 8c,e) was observed on the surface of the colorant layer, which partially penetrated into the layer itself. The colorant layer was enriched with silicon (Figure 8f), calcium (Figure 8e) and phosphorus (Figure 8g), while the last two elements were not observed in the rock substrate. The substrate of rock panel was enriched with petrogenic elements such as silicon (Figure 8f), aluminum (Figure 8d) and sodium (Figure 8h), which were probably derived from feldspars. Small iron-containing (Figure 8i) particles were observed on the surface of the colorant paint layer, but under the gypsum encrustations.

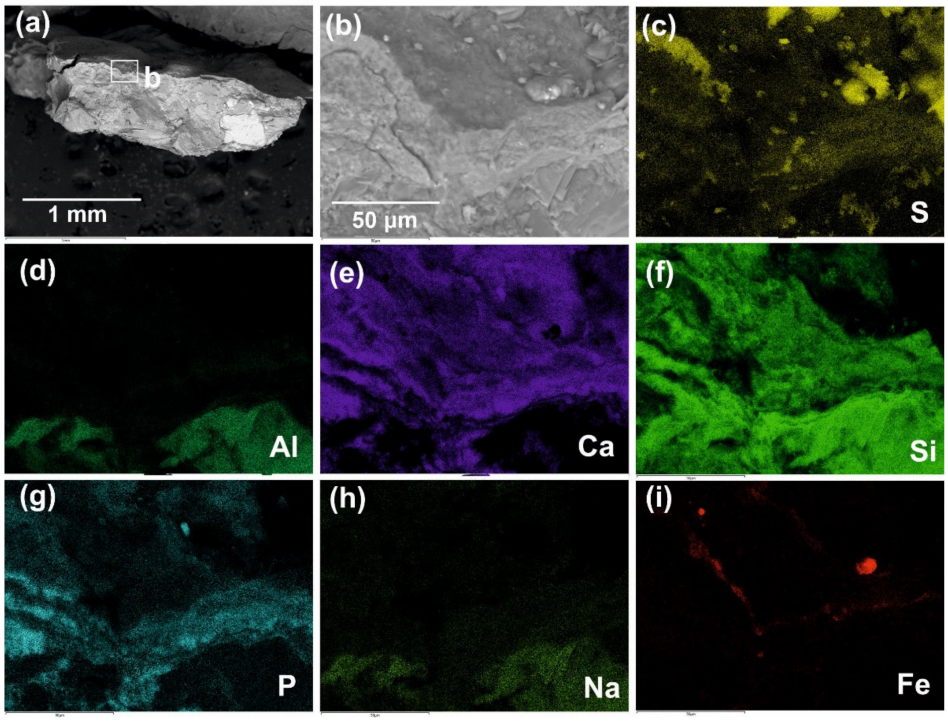

Figure 8. BSE images and elemental maps for the colorant from the Zmiev Kamen' pictograph: (**a**) BSE image of the cleavage perpendicular to the colored surface; (**b**) magnified b site; (**c**–**i**) elemental maps for S, Al, Ca, Si, P, Na and Fe, respectively.

The surface of the colorant layer had a multilayer structure containing bubbles (Figure 9a,b) probably related to the application of colorant onto the rough surface of the rock panel. The collapsed (or dried and peeled off) bubbles result in a layered circular surface structure. The particles of iron-containing compound (hematite identified by Raman spectroscopy, Figure 10) were located along the periphery of the bubbles (Figure 9e), which possibly indicates their sliding down over the spherical bubble surface to the bottom in the process of settling and drying. Calcium sulfates identified by Raman spectroscopy as gypsum (Figures 9g and 10) were randomly distributed across the surface. The colorant layer was enriched with silicon (Figure 9h), calcium (Figure 9d), phosphorus (Figure 9f) and aluminum (Figure 9c), which may indicate a mixture of quartz, clay substance, apatite, calcite and iron-containing substance. The presence of apatite was confirmed by Raman spectroscopy with the band of the $\nu_1(PO_4)$ vibration at ~960 cm^{-1} (Figure 10). Moreover, two broad carbon bands at 1338 and 1558 cm^{-1} were observed in the colorant, indicating that the red coloring pigment of the Zmiev Kamen' pictograph comprises a mixture of two components—hematite and bone black.

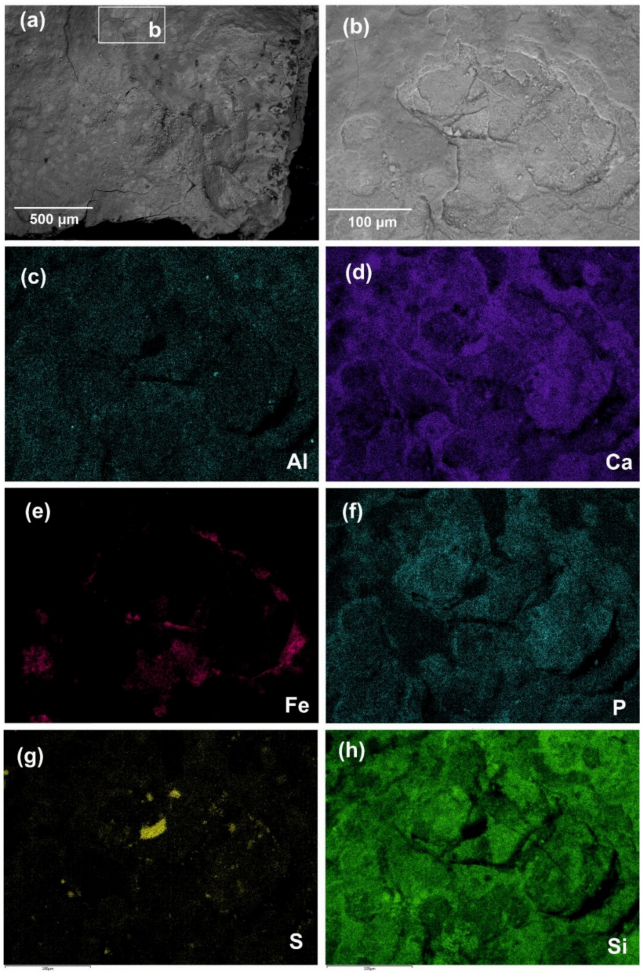

Figure 9. BSE images and elemental maps of the colorant from the Zmiev Kamen' pictograph: (**a**) BSE image of the colored surface; (**b**) magnified b site; (**c**–**h**) elemental maps for Al, Ca, Fe, P, S and Si, respectively.

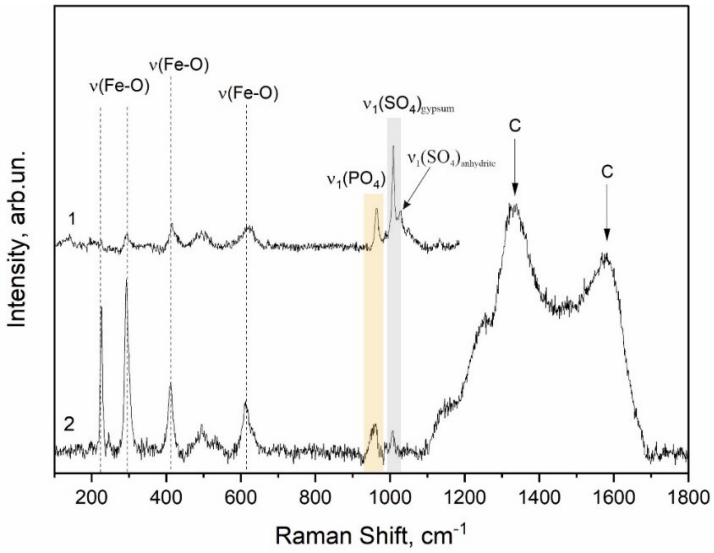

Figure 10. Raman spectra of the red colorant from the Zmiev Kamen' pictograph: 1—red colorant on the perpendicular cleavage; 2—red colorant on the surface.

3.4. Chromatographic Analysis of the Organic Phase of Colorants

The results of the chromatographic analysis of the organic phase of colorants and corresponding rock substrates are given in Table 1. For the colorant from the Idrisovskaya II pictograph, the extracts obtained were not sufficient to provide appropriate analytical signals due to the rather small size of the analyzed fragment. The data in Table 1 refers to the methyl esters of fatty acids, while the formulae and common and trivial names for fatty acids are given for convenience. The identification of sample components was carried out using mass spectra obtained in the TIC (total ion current) mode with further SIM (selected ion monitoring) of $m/z = 74$ for the most intense ions in the mass spectrum of the methyl esters of fatty acids. For comparative purposes, the fatty acid composition is given as mass-normalized SIM (selected ion monitoring at $m/z = 74$) intensities (peak areas). This ion is characteristic for all saturated and monoenoic fatty acids. The selected ion monitoring of $m/z = 74$ allowed the instrument to be used in its most sensitive mode, providing the highest signal-to-noise ratio.

Table 1. Mass-normalized SIM fatty acid intensities (peak areas) in the colorants from the Zmiev Kamen' pictograph and Ignatievskaya cave and corresponding rock substrates.

Figure	Systematic Name	Trivial Name	Ignatievskaya Cave Colorant	Ignatievskaya Cave Rock Substrate	Zmiev Kamen' Colorant	Zmiev Kamen' Rock Substrate
C14:0	Tetradecanoic	Myristic	1052429	n/a	24304	5853
iC15:0	Isopentadecanoic		n/a	n/a	14397	n/a
C15:0	Pentadecanoic		828714	n/a	9382	n/a
iC16:0	Isohexadecanoic	Isopalmitic	n/a	n/a	80349	n/a
C16:0	Hexadecanoic	Palmitic	7983571	n/a	400879	31461
C17:0	Heptadecanoic	Margaric	227143	n/a	n/a	n/a
C18:0	Octadecanoic	Stearic	1384571	n/a	226199	15962
C20:0	Eicosanoic	Arachidic	n/a	n/a	7601	n/a
16:1 *cis*-7	*cis*-7-Hexadecenoic	Hypogeic	623429 *	n/a	n/a	n/a
16:1 *cis*-9	*cis*-9-Hexadecenoic	Palmitoleic	n/a		2787050 *	
18:1 *cis*-9	*cis*-9-Octadecenoic	Oleic	496143 *	n/a	14917149 *	n/a
Sample mass, g			0.007	0.0092	0.7325	0.9434

* Fatty acids determined in the total ion current (TIC) mode.

According to the results of the chromatographic analysis, both colorant samples contained primarily saturated even-chain palmitic *C*16:0 (P) and stearic *C*18:0 (S) fatty acids, including lower amounts of myristic *C*14:0 (*M*) and saturated odd-chain pentadecanoic (C15:0) acid.

Monounsaturated fatty acids (MUFA) were found in the colorant samples: cis-7-hexadecenoic (hypogeic) and cis-9-octadecenoic (oleic) acids in the colorant from the Ignatievskaya cave, as well as cis-9-hexadecenoic (palmitoleic) and cis-9-octadecenoic (oleic) acids in the colorant from the Zmiev Kamen' pictograph. The MUFA were observed in the total ion count (TIC) mode.

The red colorant from the Ignatievskaya cave was characterized by the presence of saturated odd-chain *C*17:0 margaric fatty acid, while the red colorant from the Zmiev Kamen' pictograph contained the isomers of fatty acids (iC15:0 isopentadecanoic and iC16:0 isopalmitic acids) and even-chain C20:0 arachidic fatty acid.

While no fatty acids were found in the rock substrate from the Ignatievskaya cave, the rock substrate of the Zmiev Kamen' contained primarily saturated even-chain palmitic, stearic and myristic fatty acids. However, their mass-normalized intensities were 4–14 times lower than in the corresponding colorant.

4. Discussion

The results of microanalytical study of the mineral and elemental composition of colorants demonstrated that the principal component of the red colorants from the Ignatievskaya cave and the Idrisovskaya II and Zmiev Kamen' pictographs was hematite. The set of characteristic bands of the Fe-O vibration in hematite at 225, 245, 290, 412, 500 and 611 cm^{-1} was registered in the Raman spectra (Figures 4, 7b and 10). No bands corresponding to other possible iron oxides such as magnetite (310, 540 and 665–670 cm^{-1}) and hydroxides such as goethite (244, 299, 385, 480, 548 and 681 cm^{-1}) were observed in the spectra [35,36]. Hematite was also found in the red colorant from the Dvuglazy Kamen' (Two-Eyed Stone) pictograph (Neyva River, Middle Urals) studied earlier [6].

However, the line broadening in the hematite spectra observed for the red colorants from the Ignatievskaya cave and the Idrisovskaya II pictograph (Figures 4a and 7b) indicates local disorder possibly correlated to the insertion of substituting ions (Al^{3+} or Ti^{2+}) into the $Fe(O)_6$ octahedra constituting hematite structure [37]. Titanium was apparently derived from the ancient gabbroids and gabbronorites (1390 to 1350 Ma) of the ultramafic-mafic layered intrusions of the Kusa-Kopan complex and associated large magmatic deposits of ilmenite and Ti-magnetite ores located 100 km further east [38]. Although the comparison of Ti and Fe maps in Figure 3 supports Ti-for-Fe substitution in hematite for the colorants from the Ignatievskaya cave and the Idrisovskaya II pictograph, it was rather difficult to define the Ti/Fe ratio due to the surface roughness of the unpolished samples. Moreover, there were some more factors responsible for the irregularities of the crystalline arrangement of hematite, such as heat treatment, grinding, biodegradation and weathering [39]. Thus, the Raman spectrum of the apparently weathered reference hematite found in the excavations at the Idrisovskaya cave was characterized by the line broadening similar to that of red colorants. The sub-micrometer sizes of Fe-bearing pigments demonstrated in BSE images and EDS maps (Figures 2, 3, 5, 6, 8 and 9) can also result in local disordering and line broadening.

Although many authors report rapid transformations of iron oxides during Raman analysis due to the in situ laser irradiation effects (such as heating and oxidation), the data on the laser powers used to avoid such effects are quite controversial. While some recommend that measurements should be performed at the lowest possible laser power of 0.01–0.5 mW [12,35,36,39], others demonstrate that hematite bands in the spectra of maghemite (γ -Fe_2O_3) and magnetite (Fe_3O_4) begin to appear when the laser power is increased above 15–20 mW [40,41]. The laser power applied in our studies was below 10 mW when excited by 488 nm and below 5 mW when excited by 633 nm, respectively, which could not promote substantial processes of phase transition and/or oxidation. In general, this corresponded to the laser powers used for the Raman spectroscopy of rock art (0.1–10 mW) [5,14,15,42] not affecting the signal quality of other informative bands in the Raman spectra.

The red pigment of the Zmiev Kamen' pictograph as composed of two components, hematite and black carbon, which were confirmed by Raman spectroscopy (Figure 10). The band at 1338 cm^{-1} corresponded to the stretching vibrations in the planar graphite structure and the band at 1558 cm^{-1} appeared as a result of defects of graphite structure and the presence of heteroatoms [12,43]. These relatively broad bands suggested that the crystallite size of the black pigment was small and the broadening of peaks indicated the high degree of disorder. The band of the $\nu_1(PO_4)$ vibration at ~960 cm^{-1} observed in the spectrum indicated the possible use of calcinated bones (bone black) as black pigment. H. Gomes et al. [12] observed the combination of carbon and iron oxides in the red colorant from the rock art paintings in Gode Roriso (Ethiopia), and indicated the thermal treatment of the hematite with a carbonaceous material resulting in the partial reduction of iron (III) oxide to iron (II) oxide by carbon, which was confirmed by the presence of hematite and magnetite and carbon bands in the Raman spectra of the red colorant.

Since no reduced forms of iron were found in the studied pigments, it was not possible to reliably ascertain if the raw material for pigment was hematite or goethite, whether

the process of heating (if any) took place in an oxidizing or reducing atmosphere, or whether the hematite and bone black powders were mixed with each other in the absence of heating. However, taking into account the finds of hematite pieces in the excavations of the Idrisovskaya cave and the overall availability of hematite from the nearby supergene deposits characterized by the presence of oxidized iron deposits (so-called "iron hats") and the iron deposits of the Alapaevsk type (hematite–limonite ores and pisolitic iron ores) in the Southern and Middle Uralian regions under consideration [6], we can assume that no heating was needed in order to obtain the bright red pigment.

We compared the obtained results with the earlier data on ICP-MS microelement and phase mineral composition and thermal analysis of the red colorant for the Zmiev Kamen' pictograph [3]. The results of the phase mineral analysis (powder X-ray diffraction) of powdered samples of rock panel with red colorant were as follows, wt.%: crystal quartz 15–20%; gypsum < 5%; calcite < 5%; clay minerals (chlorite and/or hydrous micas) 5–10%; amphibole (up to 50% of hornblende confirmed by the endothermic effect at 1174 °C) [3]. This was in a rather satisfactory agreement with the results of SEM-EDS and Raman spectroscopy. However, no significant amounts of iron minerals (as well as bone apatite) were found either by XRD or ICP-MS, which supports a conclusion about the minor role of iron minerals in the preparation of colorants [3]. Indeed, the iron content in the red colorant of the Zmiev Kamen' pictograph observed in the present study was visually lower than in the red colorants from the Ignatievskaya cave and Idrisovskaya II pictograph (see Fe elemental maps in Figures 2c, 3d, 5f, 6, 8i and 9e), possibly due to the mixing with black carbon pigment. Although Fe mineral phases were below the limits of detection by XRD (0.61–0.78 wt.% of Fe as determined by ICP-MS) [3], Raman spectroscopy is sufficiently sensitive to reveal the peaks of Fe-O vibrations in hematite (and P-O vibrations in apatite) even following dilution with bone black; the iron content in the resulting pigment is sufficient for the red color to persist in the colorant. However, the distribution of iron across the surface of colorant and its confinement to the circular areas of peeled colorant layers points to the repeated application of an iron-containing substance rather than the natural distribution of Fe-containing mineral grains (see for comparison the black pigment of the Ignatievskaya cave, Figure 3d). The fairly low mass losses of organic matter in the red colorant determined by thermal analysis in the temperature range of 250–500 °C (0.5–0.9 wt.%) [3] were consistent with the presence of inorganic compounds and bone black in the colorant.

Earlier, V.S. Zhitenev identified the composition of the red colorants from the Ignatievskaya cave by SEM-EDS, XRF spectrometry and X-ray diffraction as quartz, calcite and clay minerals, along with traces of gypsum and insignificant content of iron, and suggested the use of feldspar as an extender [24]. We suppose that the quartz, calcite and feldspar (Figure 2c) originated from the rock panel rather than comprising an artificial addition to the colorant, while the gypsum was more of an authigenic mineral, i.e., forming crystal encrustations on the rock and colorant surface (Figure 8). This was clearly demonstrated by the underlying rock panel composed of calcite and dolomite (Figures 5d–f and 6) for the colorant from the Idrisovskaya II pictograph. The feldspar was distributed across the colorant surface in the form of rare individual grains (Figures 2c and 3d) in sufficiently small amounts as to preclude the likelihood of its artificial addition in high amounts as an extender.

The fine-grained (<1–5 μm in size) hydromicous mineral containing iron (hematite) found in the red colorants apparently could originate from the mixing of hematite particles with clayey extender for the Ignatievskaya cave and Idrisovskaya II pictographs, and with addition of bone black into the colorant mixture for the Zmiev Kamen' pictograph. Thus, the presence of iron minerals as inorganic pigments in red colorants was confirmed; the rather small amounts can be possibly explained as due to mixing with the clayey extender in order to achieve the desired hue. Even such small amounts of hematite possess strong coloring properties to provide the bright color to the masterworks of parietal art.

The principal pigment in the black colorant of the drawings from the Ignatievskaya cave was carbon, as confirmed by the Raman spectroscopy. The absence of Raman bands attributable to organic residuals indicated that the black pigment was fully fired in a reducing atmosphere [12,43]. Moreover, the absence of phosphate functional group at 960 cm^{-1} in the Raman spectrum (Figure 4), which excluded the use of calcinated bones (bone black) in preparing the black pigment (Figure 5), rather suggested the use of charcoal of vegetal origin; this was supported by the finds of charcoal pieces during excavations carried out in the Ignatievskaya cave [25,26,29].

Authigenic minerals that form in situ within the cave sediments, as opposed to those that are transported into the cave, can be used to reconstruct the ancient chemical environments in the sediments [44]. Each mineral forms under a specific set of conditions, and hence its presence is indicative of the conditions that prevailed at the time of formation.

Bicarbonate waters equilibrated with carbonate host rocks of the caves drain the sediments over long periods of geological time to move the water–rock equilibria toward a higher alkalinity of pH = 7.0–8.5, favoring the stabilization of carbonates [45] in the form of speleothems (stalactites and stalagmites, moon milk) (Figure 4b,e).

Phosphates, which are among the most common, widespread and manifold authigenic minerals (about sixty mineral species), form by interaction of clayey matter, aluminous silicate rocks and/or limestone with solutions enriched in phosphate derived from bat or bird guano during its bacterial and fungal degradation [44,45]. Since many of the authigenic phosphates have relatively poor order at the atomic level, and/or very small crystal sizes and irregular distribution across the surface [44], they are not easily detected by Raman spectroscopy. For this reason, scanning electron microscopy and elemental analyses using an energy dispersive spectrometer can be of great assistance.

Thus, phosphorus distribution across the P elemental maps in the colorants from the Ignatievskaya cave (Figure 3d) might be connected with the formation of Ca-bearing phosphates such as crandallite $CaAl_3(PO_4)_2(OH)_5 \cdot H_2O$; ardealite $Ca_2(SO_4)(HPO_4) \cdot 4H_2O$; brushite $CaHPO_4 \cdot 2H_2O$; whitlockite $Ca_9(Mg,Fe^{2+})(PO_4)_6(HPO_4)$; montgomeryite Ca_4 $(Mg,Fe)Al_4(PO_4)_6$ $(OH)_4 \cdot 12H_2O$ and dahllite $Ca_5(PO_4,CO_3)_3(OH)$, or K,Na,Al-bearing phosphates such as taranakite $(K,Na,NH_4)_3(Al,Fe^{3+})_5(HPO_4)_6(PO_4)_2 \cdot 8H_2O$); leucophosphite $(KFe^{3+}{}_2(PO_4)_2$ $(OH) \cdot 2H_2O)$; tinsleyite $K(Al,Fe)_2(PO4)_2(OH) \cdot 2H_2O$ and variscite $Al(PO_4) \cdot 2H_2O$ [44,45]. Ardealite, a sulfate phosphate $(Ca_2(SO_4)(HPO_4) \cdot 4H_2O)$, may form early during the process in limestone of dry caves and sometimes coexists with gypsum $(CaSO_4 \cdot 2H_2O)$ [45].

Similar to their formation in cave environments, authigenic phosphates may form on the rock surfaces exposed to the impact of atmospheric factors, such as humidity, temperature, dust and sunlight. Phosphorus from soil and, to a lesser extent, bird excrements can produce phosphate-enriched media resulting in the formation of phosphates. Moreover, the apatite from the bone black in the red colorant from the Zmiev Kamen' pictograph could have been an additional source of phosphorus.

The whitish substance filling the micro-cracks on the surface of red colorant from the Idrisovskaya II pictograph was identified as $Ca(C_2O_4) \cdot 2H_2O$ weddellite (Figure 7a). The calcium oxalate minerals whewellite $Ca(C_2O_4) \cdot H_2O$ and weddellite $Ca(C_2O_4) \cdot (2 + x)H_2O$ are common on rock surfaces and may encapsulate and stabilize the paints of pictographs, protecting them from weathering and fixing the colorants on the rock panel [4,5,13,15,46]. Oxalates are generally associated with prehistoric pictographs but also exist on natural rock outcrops, both those in open air and protected from atmospheric precipitation surfaces.

The origin of whewellite and weddellite on exposed surfaces is not fully understood. Proposed sources include natural processes such as biological activity of organisms living on or within the stone, reactions of organic compounds in rain or aerosols at the atmosphere/rock boundary, as well as reactions and/or deposition of dissolved organic matter in runoff, and animal urine [4,5,13,15,46].

Earlier weddellite has been found in another open-air pictograph, Dvuglazy Kamen' (Neyva River, Middle Urals) whose rock massive is composed of silicified limestone [6]. Although the substrates on which oxalates are known to occur include granite, marble,

limestone and sandstone, no weddellite has been observed in the colorant of the Zmiev Kamen' pictograph granite rock panel.

One of the principal reasons for oxalate formation can be the presence of lichens— symbiotic associations of fungi (mycobionts) and microscopic green algae and/or cyanobacteria (photobionts)—which can be highly rock-specific, like the lichen calcareus L. *Aspicilia calcarea* (L.), and produce pruina (a wax-like protective coating made of weddellite) [4,6,13]. Here, the possible lithobiontic community could be made up of a great variety of microorganisms, lichens, and cyanobacteria [47]. Their traces were clearly visible on the rock surface of the Idrisovskaya II pictograph (Figure 11).

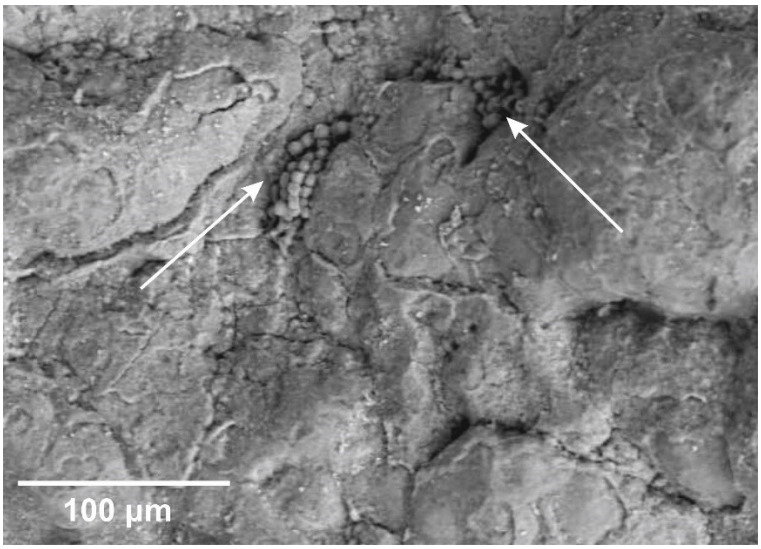

Figure 11. BSE image of the fragment of the red colorant from the Idrisovskaya II pictograph demonstrating the aggregates of spherical particles (apparently cyanobacteria) on the surface depressions (marked by arrows).

All studied sites (both cave and open-air) were characterized by the formation of authigenic gypsum as encrustations covering the colorant layer (Figures 3c, 4c, 6, 8c and 10). Several possible mechanisms of gypsum formation on the limestone surface are described: (i) gypsum crystallization due to the evaporation of sulfate-rich pore waters percolating through the limestone strata; (ii) sulfur oxide migration from the dry and wet atmospheric precipitation (probably predominating mechanism for open-air pictographs); and (iii) artificial application of sulfur-containing organic compounds with the binder of colorant (tallow or bone marrow) [6,16].

The phosphate assemblages can coexist with gypsum in caves [45,48]. Since the process of phosphoritization of the organic remains present in the unconsolidated deposits (bone detritus, bat guano and coprolites) in the Ignatievskaya cave was accompanied by the acidification of the environment, the reaction of H_2SO_4 with carbonate substrate resulted in the formation of gypsum [48]. The subaerial phosphorite-gypsum deposits in the Ignatievskaya cave indicate the relatively warm conditions of the arid Mikulian Interglacial climate [48].

Moreover, $CaSO_4$ anhydrite is identified in the Raman spectrum of the red colorant from the Zmiev Kamen' (Figure 10). The simultaneous presence of easily hydrated–dehydrated minerals such as gypsum $CaSO_4 \cdot 2H_2O$ and anhydrite $CaSO_4$, as well as whewellite $Ca(C_2O_4) \cdot H_2O$ and weddellite $Ca(C_2O_4) \cdot (2 + x)H_2O$, may indicate the alternation of dry and wet climatic conditions during the formation of oxalate and gypsum encrustations over the rock surface for open-air pictographs [13,15]. However, for the Ignatievskaya cave, with its rather stable temperature and humidity regime (t = 5.0 °C and f = 99% in summer, t = 3.5° C and f = 78% in winter, and t = 6.0 °C and f = 99% in autumn), this seems highly unlikely [48].

The absence of Raman bands attributable to organic residuals in studied colorants indicates the significant degree of its decomposition and structural transformation. Thus, based on the results of the chromatographic analysis of fatty acids, which was ultrasensitive to the organic remains, we have attempted to evaluate the organic composition of red colorants.

The recipes of prehistoric paintings most frequently include organic binders of vegetable or animal origin such as plant juices or oils, urine, animal fat, bone marrow, blood, eggs (yolk and/or albumen), as well as human saliva, in order to form a stable, homogeneous, flexible and viscous paste with the pigment and extender [4,7,16,18–20]. The basis of such binders is generally composed of proteinaceous, lipidic, glucidic (plant gums) or waxy (beeswax) materials. H. Gomes et al., found the remains of beeswax in the white colorant from the rock art paintings in Gode Roriso (Ethiopia) [12].

Triglycerides are the main form of lipids in living organisms and consist of a glycerol molecule combined with three fatty acids, comprising esters of glycerin with saturated and unsaturated fatty acids in long linear chains [49]. Lipids are sensitive to chemical and biological alteration processes; for example, hydrolytic degradation releases fatty acids from triacylglycerols and β-oxidation, while reduction processes lead to the loss of unsaturated acids [19,49,50]. In most of the archaeological pigment samples, the main components of the residual organic phase are comprised of free fatty acids and their salts, indicating that the originally present triacylglycerols underwent hydrolysis and reacted with the mineral matrix of the samples [19].

Despite the large number of naturally occurring fatty acids (more than 1000), only some of them were found in significant quantities. The most common saturated fatty acids of both animal and plant origin were unbranched carbon chain compounds containing 16 and 18 carbon atoms: palmitic (C16:0) and stearic (C18:0) acids, which are most often preserved in organic residues, since unsaturated fatty acids are quite easily decomposed [19,49,50]. Given that short- and medium-chain fatty acids arising from oxidation processes are more soluble in percolating ground water than long-chain fatty acids, degraded lipids in archaeological samples are identified by high concentrations of palmitic (C16:0) and stearic (C18:0) acids [19].

Since no fatty acids were found in the rock substrate of the painting from the Ignatievskaya cave, taphonomic contamination of the colorant can be excluded. The fatty acid distributions with a greater abundance of palmitic acid (C16:0) than stearic acid (C18:0), together with minor oleic acid (C18:1) obtained for the colorant (Table 1), are typical of degraded animal fats [19,20]. The presence of odd-carbon-numbered, straight-chain components—specifically C15:0 and C17:0—point to a ruminant origin [51].

The use of the P/S ratio (ratio of mass fractions of palmitic and stearic acids) proposed to discriminate fatty substances by their origin [6,51–53] is debated in the literature due to their high concentration either in plant or in animal sources; moreover, the significant amounts of C16:0 and C18:0 FAs could also be the result of the conversion of unsaturated FAs to SFAs [23,54]. Thus, only a combination of criteria including fatty acids distribution, abundances of minor components, such as odd-carbon number branched-chain fatty acids, and positional isomers of unsaturated compounds, enables distinctions to be made among different types of animal fats [23]. Based on the concept that further FFAs or different ratios could provide a more reliable and accurate identification strategy, the following ratio (C15:0 + C17:0)/(C12:0 + C14:0 + C16:0 + C18:0) was proposed for discriminating between monogastric (<0.04) and ruminant (> 0.04) animal fats residues [55,56].

The calculated ratio (C15:0 + C17:0)/(C12:0 + C14:0 + C16:0 + C18:0) for the organic fraction of the red colorant from the Ignatievskaya cave was equal to 0.10, indicating the presence of ruminant fat. However, the ratios of palmitic to stearic (P/S) and palmitic to myristic (P/M) acids calculated for the colorant from the Ignatievskaya cave were P/S = 5.8 and P/M = 7.6, which are quite atypical for adipose and dairy fats known for domesticated ruminants [53]. A comparison with the bone marrow from the metatarsal bones of wild ruminants—European fallow deer (P/S = 5.5 and P/M = 6.7) [57], North American elk

and mule deer (P/S = 4.4 − 3.5 and P/M = 7.7 − 19.4) [58]—demonstrated that binder for the red pigment could have originated from the bone marrow of wild ruminants like roe deer, moose or other members of the deer (*Cervidae*) family. The use of bone marrow of guanaco from Patagonia was suggested in the archaeological pigment residues from one of the most remote regions of the planet (Beagle Channel region, Tierra del Fuego, Southern South America) [19].

Since forming the components of the cellular membranes of autotrophic bacteria, the presence of monounsaturated fatty acids in the red colorant from the Ignatievskaya cave may be due to the activity of the cave bacterial communities, such as sulfur and sulfide oxidizers, iron and manganese oxidizers, sulfate reducers, as well as nitrifiers, that appear to be abundant in cave environments [59]. These bacteria play a significant role in the dissolution of limestone in caves with hydrogen sulfide-rich waters, contributing to cave enlargement, as well as having possible biocorrosive potential to cause irreversible damage to the rock art paintings due to the degradation and discoloration of painting pigments [59].

The cis-7-hexadecenoic (hypogeic) acid has been isolated from the strains of the genus *Nitrospira*, a kind of nitrite oxidizing autotrophic bacteria [60]. Such bacteria have been found among the bacterial communities on Paleolithic paintings and surrounding rock walls in two Spanish caves (Llonín and La Garma) [59].

Although the substrate of the Zmiev Kamen' pictograph contained myristic, palmitic and stearic acids, their content was rather low to significantly affect the fatty acid composition of corresponding red pigment. Moreover, the substrate lacked MUFA (palmitoleic and oleic acids), saturated odd-chain pentadecanoic (C15:0) and even-chain (C20:0) arachidic fatty acids, as well as branched-chain fatty acids (iC15:0 isopentadecanoic and iC16:0 isopalmitic) found in the colorant. This difference suggests that the presence of organic fraction in the colorant was not the result of taphonomic contamination.

The branched-chain fatty acids and MUFA are well known as bacterial markers [19,51]. As discussed above, the presence of microorganisms within the lithobiontic communities inhabiting the rock surfaces of open-air pictographs is quite common. However, these compounds also occur in the fats of ruminant animals.

The calculated ratio (C15:0 + C17:0)/(C12:0 + C14:0 + C16:0 + C18:0) for the organic fraction of the red colorant from the Zmiev Kamen' pictograph was equal to 0.01, which indicates the presence of monogastric animal fat. Moreover, it corresponded to the ratio (0.01) obtained for the experimental rock painting drawn with ground ochre mixed with pig lard on a stone in 1992 and left in a grotto near the Dvuglazy Kamen' pictograph (Neyva River, Middle Urals, Russia) and analyzed in 2021 [6].

5. Conclusions

Studies of mineral, elemental and organic phase composition of the colorant microsamples from the drawings of Ignatievskaya cave and Idrisovskaya II and Zmiev Kamen' pictographs (Southern and Middle Urals, Russia) were carried out using a set of microspectroscopic methods with high spatial resolution (SEM-EDS and Raman spectroscopy). The fatty acid composition of the organic phase was analyzed by GC–MS following methylation.

The red colorants were characterized by the presence of fine-grained (< 1–5 μm in size) hydromicous mineral containing iron, apparently originating from the thorough grinding and mixing of hematite particles with clayey extender for the Ignatievskaya cave and Idrisovskaya II pictographs, and the addition of bone black into the red colorant mixture for the Zmiev Kamen' pictograph. The principal pigment in the black colorant of the drawings from the Ignatievskaya cave was charcoal of vegetal origin. No traces of thermal treatment were found for inorganic pigment (hematite).

The proportions of fatty acids derived from the colorants corresponded to monogastric animal fat (possibly pig (boar) adipose tissue (lard) for the red colorant from the Zmiev Kamen' pictograph) and ruminant fat (possibly bone marrow) for the red colorant from the Ignatievskaya cave), which could well have been added into the colorant mixture as an organic binder.

The technology of colorant manufacture likely involved thorough grinding and mixing of hematite with an organic binder of animal origin and clayey extender in order to achieve the desired hue and intensity when applying the colorant in layers (Idrisovskaya II and Zmiev Kamen' pictographs).

The development of authigenic phosphate mineralization is inherent both to cave- and open-air sites resulting in the formation of a number of Ca-bearing and K,Na,Al-bearing phosphates due to the availability of phosphorus released in the process of bat/bird guano—or, less commonly, bone biodegradation—to produce acid solutions enriched in phosphate that dissolve limestone and apatite.

All studied sites (both cave and open-air) were characterized by the formation of authigenic gypsum in the form of encrustations covering the colorant layer. In the Ignatievskaya cave the phosphoritization of the organic remains in the unconsolidated deposits (bone detritus, bat guano and coprolites) was accompanied by the acidification of environment and gypsum crystallization. In the case of the open-air pictographs, gypsum forms as a result of migrations of sulfur oxides with dry and wet atmospheric precipitation and limestone and granite dissolution. Moreover, the sulfur from organic binder (S-enriched triglycerides from adipose fat and bone marrow) and activity of sulfur oxidizing bacteria could be the additional source for gypsum crystallization in all colorants.

The activity of autotrophic cave and lithobiontic microbial communities (and sulfate reducers, nitrifiers, etc.) was observed even on areas visually free from bacterial colonies. Evidence of calcium oxalate encrustation, formed as a result of the biological activities of microorganisms (lichens, cyanobacteria) from the lithobiontic community of limestone rock, was found in the images of the Idrisovskaya II pictograph. Although no oxalates were found on its surface, the presence of lithobiontic microorganisms on the granite substrate of the Zmiev Kamen' pictograph, as confirmed by GC–MS, demonstrated the high specificity of certain microorganisms to rock composition.

The simultaneous presence of easily hydrated–dehydrated minerals, such as gypsum and anhydrite (Zmiev Kamen' pictograph), and calcium oxalates (Idrisovskaya II pictograph) indicated the alternation of dry and wet climatic conditions during the formation of mineral encrustations covering the rock surface of open-air pictographs, while the cave environment was more generally characterized by highly stable temperature and humidity regimes.

Author Contributions: Conceptualization, D.K. and V.S.; sample collection, V.S. and E.S.; Raman analysis, E.P.; SEM-EDS analysis, E.S.; GC–MS analysis, A.K. and D.D.; writing—original draft preparation, D.K.; data curation, E.P. and E.S.; writing—review and editing, D.K.; visualization, E.S. and E.P.; project administration, D.K.; funding acquisition, D.K. All authors have read and agreed to the published version of the manuscript.

Funding: This research was funded by the Russian Science Foundation, grant number 22-18-00593.

Institutional Review Board Statement: Not applicable.

Informed Consent Statement: Not applicable.

Data Availability Statement: The data presented in this study are available on request from the corresponding author.

Acknowledgments: The authors are grateful to Danila K. Dubrovsky (OOO "Grachev and Partners", Ekaterinburg) for providing the samples from the Zmiev Kamen' pictograph. The authors wish to thank Thomas Beavitt for providing linguistic support and proofreading the article.

Conflicts of Interest: The authors declare no conflict of interest. The funders had no role in the design of the study; in the collection, analyses, or interpretation of data; in the writing of the manuscript; or in the decision to publish the results.

References

1. Shirokov, V.N.; Chairkin, S.E. *Rock Paintings of the Northern and Middle Urals*; Azhur Publishing House: Ekaterinburg, Russia, 2011; p. 181. (In Russian)
2. Bersani, D.; Lottici, P.P. Raman spectroscopy of minerals and mineral pigments in archaeometry. *J. Raman Spectrosc.* **2016**, *47*, 499–530. [CrossRef]
3. Shirokov, V.N.; Dubrovsky, D.K.; Surikov, D.V.; Kiseleva, D.V.; Petrishcheva, V.G. Rock paintings of the Middle and Southern Urals: Microelement composition of samples of ancient paints. *Ural. Istor. Vestn.* **2014**, *1*, 100–111. (In Russian)
4. Hernanz, A.; Gavira-vallejo, J.M. Chapter 10. Rock Art. In *Analytical Strategies for Cultural Heritage Materials and their Degradation*; The Royal Society of Chemistry: London, UK, 2021; pp. 201–226. [CrossRef]
5. Hernanz, A.; Ruiz-López, J.F.; Madariaga, J.M.; Gavrilenko, E.; Maguregui, M.; Fdez-Ortiz de Vallejuelo, S.; Martínez-Arkarazo, I.; Alloza-Izquierdo, R.; Baldellou-Martínez, V.; Viñas-Vallverdú, R.; et al. Spectroscopic characterisation of crusts interstratified with prehistoric paintings preserved in open-air rock art shelters. *J. Raman Spectrosc.* **2014**, *45*, 1236–1243. [CrossRef]
6. Kiseleva, D.V.; Shirokov, V.N.; Shagalov, E.S.; Pankrushina, E.A.; Danilov, D.A.; Khorkova, A.N. Comparative analysis of the modern and ancient coloring pigment in the paintings from the Two-eyed stone (Dvuglazyi Kamen') pictograph (the Neyva river, the Middle Urals). *Nanotechnol. Russ.* **2021**, *16*, 676–683. [CrossRef]
7. Pozo-Antonio, J.S.; Comendador Rey, B.; Alves Bacelar, L.; Barreiro, P. Methodological approach (in situ and laboratory) for the characterisation of late prehistoric rock Paintings—Penedo Gordo (NW Spain). *Minerals* **2021**, *11*, 551. [CrossRef]
8. Pakhunov, A.S.; Svetogorov, R.D.; Ovcharov, A.V.; Shushunov, M.N.; Senin, R.A. Analysis of ochre samples from the cultural layer of the chamber of signs at the Kapova cave. *Ross. Arheol.* **2021**, *1*, 18–30. [CrossRef]
9. Pakhunov, A.S.; Devlet, E.G.; Karateev, I.A.; Svetogorov, R.D.; Dorovatovskii, P.V.; Senin, R.A.; Blagov, A.E.; Yatsishina, E.B. The composition of paints of the paintings on stone cist slabs from Karakol (Altai). *Crystallogr. Rep.* **2018**, *63*, 1027–1033. [CrossRef]
10. Pakhunov, A.S.; Devlet, E.G.; Molodin, V.I.; Lazin, B.V.; Karateev, I.A.; Dorovatovsky, P.V.; Kaloyan, A.A.; Podurets, K.M.; Senin, R.A.; Blagov, A.E.; et al. A comparative analysis of paints on the Karakol burial slabs. *Archaeol. Ethnol. Anthropol. Eurasia* **2017**, *45*, 56–68. [CrossRef]
11. Pakhunov, A.S.; Zhitenev, V.S. New data on upper paleolithic paint recipes: Scientific examination of massive paint remains from Kapova Cave, Southern Ural, Russia. *Strat. Plus* **2015**, *1*, 125–135.
12. Gomes, H.; Rosina, P.; Holakooei, P.; Solomon, T.; Vaccaro, C. Identification of pigments used in rock art paintings in Gode Roriso-Ethiopia using Micro-Raman spectroscopy. *J. Archaeol. Sci.* **2013**, *40*, 4073–4082. [CrossRef]
13. Russ, J.; Kaluarachchi, W.D.; Drummond, L.; Edwards, H.G.M. The Nature of a whewellite-rich rock crust associated with pictographs in Southwestern Texas. *Stud. Conserv.* **1999**, *44*, 91–103.
14. Prinsloo, L.C.; Barnard, W.; Meiklejohn, I.; Hall, K. The first Raman spectroscopic study of San rock art in the Ukhahlamba Drakensberg Park, South Africa. *J. Raman Spectrosc.* **2008**, *39*, 646–654. [CrossRef]
15. Tournié, A.; Prinsloo, L.C.; Paris, C.; Colomban, P.; Smith, B. The first in situ Raman spectroscopic study of San rock art in South Africa: Procedures and preliminary results. *J. Raman Spectrosc.* **2011**, *42*, 399–406. [CrossRef]
16. Reese, R.; Hyman, M.; Rowe, M.; Derr, J.; Davis, S. Ancient DNA from Texas pictographs. *J. Archeol. Sci.* **1996**, *23*, 269–277. [CrossRef]
17. Rousaki, A.; Vandenabeele, P. In situ Raman spectroscopy for cultural heritage studies. *J Raman Spectrosc.* **2021**, *52*, 2178–2189. [CrossRef]
18. Brook, G.A.; Franco, N.V.; Cherkinsky, A.; Acevedo, A.; Fiore, D.; Pope, T.R.; Weimar, R.D.; Neher, G.; Evans, H.A.; Salguero, T.T. Pigments, binders, and ages of rock art at Viuda Quenzana, Santa Cruz, Patagonia (Argentina). *J. Archeol. Sci. Rep.* **2018**, *21*, 47–63. [CrossRef]
19. Fiore, D.; Maier, M.; Parera, S.D.; Orquera, L.; Piana, E. Chemical analyses of the earliest pigment residues from the uttermost part of the planet (Beagle Channel region, Tierra del Fuego, Southern South America. *J. Archeol. Sci.* **2008**, *35*, 3047–3056. [CrossRef]
20. Maier, M.S.; de Faria, D.L.A.; Boschín, M.T.; Parera, S.D.; del Castillo Bernal, M.F. Combined use of vibrational spectroscopy and GC–MS methods in the characterization of archaeological pastes from Patagonia. *Vib. Spectrosc.* **2007**, *44*, 182–186. [CrossRef]
21. Kiseleva, D.V.; Danilov, D.A.; Domracheva, D.V.; Trufanov, A.Y.; Khorkova, A.N.; Sharapova, S.V. Gas chromatography–mass spectrometry (GC–MS) study of the archaeological plant mixture from an elite burial mound of the Sargat cuture in the Middle Irtysh river basin. *Nanotechnol. Russ.* **2020**, *15*, 617–622. [CrossRef]
22. Bonaduce, I.; Ribechini, E.; Modugno, F.; Colombini, M.P. Analytical approaches based on gas chromatography mass spectrometry (GC/MS) to study organic materials in artworks and archaeological objects. *Top. Curr. Chem. Z* **2016**, *374*, 297–327. [CrossRef]
23. Regert, M. Analytical strategies for discriminating archeological fatty substances from animal origin. *Mass Spectrom. Rev.* **2011**, *30*, 177–220. [CrossRef] [PubMed]
24. Zhitenev, V.S. *S.N. Bibikov i Pervobytnaya Arkheologiya [S.N. Bibikov and Prehistoric Archaeology]*; IIMK RAN Publ.: St. Petersburg, Russia, 2009; pp. 219–223. (In Russian)
25. Petrin, V.T. *Paleoliticheskoye Svyatilishche V Ignatiyevskoy Peshchere Na Yuzhnom Urale [Palaeolithic Sanctuary in Ignatievskaya Cave in the Southern Urals]*; Nauka Press: Novosibirsk, Russia, 1992; pp. 1–207. (In Russian)
26. Shirokov, V.N.; Petrin, V.T. *Iskusstvo Lednikovogo Veka. Ignatiyevskaya I Serpiyevskaya 2 Peshchery Na Yuzhnom Urale [The Art of the Glacial Age. Ignatievskaya and Serpievskaya 2 Caves in the Southern Urals]*; Azhur Publishing House: Ekaterinburg, Russia, 2013; pp. 1–190. (In Russian)

27. Dublyansky, Y.; Kosintsev, P.; Shirokov, V.; Spötl, C. Humans in Ignatievskaya cave during the Paleolithic: Improvement and expansion of the radiocarbon chronology. *Ross. Arkheologiia* **2021**, *3*, 7–19.
28. Smirnov, N.G.; Bolshakov, V.N.; Kosintsev, P.A.; Panova, N.K.; Korobeynikov, Y.I.; Olshvang, V.N.; Bykova, G.V. *Istoricheskaya ekologiya zhivotnykh gor Yuzhnogo Urala [Historical ecology of animals of the Southern Ural Mountains]*; UrO AN SSSR: Sverdlovsk, Russia, 1990; pp. 1–224.
29. Dublyansky, Y.; Shirokov, V.; Moseley, G.E.; Kosintsev, P.A.; Edwards, R.L.; Spötl, C. ^{230}Th dating of flowstone from Ignatievskaya Cave, Russia: Age constraints of rock art and paleoclimate inferences. *Geoarchaeology* **2021**, *36*, 532–545. [CrossRef] [PubMed]
30. Steelman, K.; Rowe, M.; Shirokov, V.; Southon, J. Radiocarbon dates for pictographs in Ignatievskaya Cave, Russia: Holocene age for supposed Pleistocene fauna. *Antiquity* **2002**, *76*, 341–348. [CrossRef]
31. Shirokov, V.N. Ignatievskaya cave: The skill of glacial century in danger. *Probl. Hist. Philol. Cult.* **2019**, *2*, 105–115.
32. Shirokov, V.N. *Ural'skiye Pisanitsy. Yuzhnyy Ural [Ural Petroglyphs. Southern Urals]*; AMB Publisher: Ekaterinburg, Russia, 2009; pp. 1–33. (In Russian)
33. Danukalova, G.; Kosintsev, P.; Yakovlev, A.; Yakovleva, T.; Osipova, E.; Kurmanov, R.; van Kolfschoten, T.; Izvarin, E. Quaternary deposits and biostratigraphy in caves and grottoes located in the Southern Urals (Russia). *Quat. Int.* **2020**, *546*, 84–124. [CrossRef]
34. Chernetsov, V.N. *Rock paintings of the Urals. Part 2 (Code of Archaeological Sources, Issues 4–12)*; Nauka: Moscow, Russia, 1971; 120p.
35. Hanesch, M. Raman spectroscopy of iron oxides and (oxy)hydroxides at low laser power and possible applications in environmental magnetic studies. *Geophys. J. Int.* **2009**, *177*, 941–948. [CrossRef]
36. Froment, F.; Tournié, A.; Colomban, P. Raman identification of natural red to yellow pigments: Ochre and iron-containing ores. *J. Raman Spectrosc.* **2008**, *39*, 560–568. [CrossRef]
37. Zoppi, A.; Lofrumento, C.; Castellucci, E.M.; Sciau, P. Al-for-Fe substitution in hematite: The effect of low Al concentrations in the Raman spectrum of Fe_2O_3. *J. Raman Spectrosc.* **2008**, *39*, 40–46. [CrossRef]
38. Shagalov, E.S.; Holodnov, V.V.; Sustavov, S.G.; Kiseleva, D.V. Cl-rich amphiboles and micas in rocks of the Middle Riphean Kusa-Kopan complex of mafic layered intrusions (Southern Urals, Russia). *Mineral. Petrol.* **2021**, *115*, 391–409. [CrossRef]
39. de Faria, D.L.A.; Lopes, F.N. Heated goethite and natural hematite: Can Raman spectroscopy be used to differentiate them? *Vib. Spectrosc.* **2007**, *45*, 117–121. [CrossRef]
40. El Mendili, Y.; Bardeau, J.-F.; Randrianantoandro, N.; Gourbil, A.; Greneche, J.-M.; Mercier, A.-M.; Grasset, F. New evidences of in situ laser irradiation effects on γ-Fe_2O_3 nanoparticles: A Raman spectroscopic study. *J. Raman Spectrosc.* **2011**, *42*, 239–242. [CrossRef]
41. Shebanova, O.N.; Lazor, P. Raman study of magnetite (Fe_3O_4): Laser-induced thermal effects and oxidation. *J. Raman Spectrosc.* **2003**, *34*, 845–852. [CrossRef]
42. Prinsloo, L.C.; Tournié, A.; Colomban, P.; Paris, C.; Bassett, S.T. In search of the optimum Raman/IR signatures of potential ingredients used in San/Bushman rock art paint. *J. Archeol. Sci.* **2013**, *40*, 2981–2990. [CrossRef]
43. Van der Weerd, J.; Smith, G.D.; Firth, S.; Clark, R.J.H. Identification of black pigments on prehistoric southwest American potsherds by infrared and Raman microscopy. *J. Archaeol. Sci* **2004**, *31*, 1429–1437. [CrossRef]
44. Karkanas, P.; Bar-Yosef, O.; Goldberg, P.; Weiner, S. Diagenesis in prehistoric caves: The use of minerals that form in situ to assess the completeness of the archaeological record. *J. Archaeol Sci.* **2000**, *27*, 915–929. [CrossRef]
45. Sokol, E.V.; Kozlikin, M.B.; Kokh, S.N.; Nekipelova, A.V.; Kulik, N.A.; Danilovsky, V.A.; Khvorov, P.V.; Shunkov, M.V. Phosphate Record in Pleistocene-Holocene Sediments from Denisova Cave: Formation Mechanisms and Archaeological Implications. *Minerals* **2022**, *12*, 553. [CrossRef]
46. Edwards, H.G.M.; Drummond, L.; Russ, J. Fourier transform Raman spectroscopic study of prehistoric rock paintings from the Big Bend region, Texas. *J. Raman Spectrosc.* **1999**, *30*, 421–428. [CrossRef]
47. Ascaso, C.; Wierzchos, J.; Souza-Egipsy, V.; de los Ríos, A.; Delgado Rodrigues, J. In situ evaluation of the biodeteriorating action of microorganisms and the effects of biocides on carbonate rock of the Jeronimos Monastery (Lisbon). *Int. Biodeterior. Biodegrad.* **2002**, *49*, 1–12. [CrossRef]
48. Chervyatsova, O.Y.; Potapov, S.S.; Parshina, N.V.; Muslukhov, S.I. Subaeral sulfate mineral formation in the Ignatievskaya cave (South Urals). *Speleol. Spelestology* **2018**, *9*, 93–99. (In Russian)
49. Dunne, J. Organic Residue Analysis and Archaeology. Supporting Information. HEAG058b. *Historic England*. 2017. Available online: https://historicengland.org.uk/images-books/publications/organic-residue-analysis-and-archaeology/ (accessed on 1 October 2022).
50. Regert, M.; Garnier, N.; Decavallas, O.; Cren-Olive, C.; Rolando, C. Structural characterization of lipid constituents from natural substances preserved in archaeological environments. *Meas. Sci. Technol.* **2003**, *14*, 1620–1630. [CrossRef]
51. Evershed, R.P.; Dudd, S.N.; Copley, M.S.; Berstan, R.; Stott, A.W.; Mottram, H.; Buckley, S.A.; Crossman, Z. Chemistry of archaeological animal fats. *Acc. Chem. Res.* **2002**, *35*, 660–668. [CrossRef] [PubMed]
52. Pozhidaev, V.M.; Sergeeva, Y.E.; Slushnaya, I.S.; Kashkarov, P.K.; Yatsishina, E.B. Application of gas-chromatography to clarify the attribution of the ancient clay vessel. *Butl. Commun.* **2017**, *52*, 73–81. (In Russian) [CrossRef]
53. Khorkova, A.N.; Danilov, D.A.; Kiseleva, D.V.; Dubyagina, E.V. Fatty acid composition of organic residue on bronze age pottery (Bozshakol, Kazakhstan) by GC–MS after acid methanolysis. In *AIP Conference Proceedings*; AIP Publishing LLC: Melville, NY, USA, 2020; Volume 2313, p. 050055. [CrossRef]

54. Irto, A.; Micalizzi, G.; Bretti, C.; Chiaia, V.; Mondello, L.; Cardiano, P. Lipids in Archaeological Pottery: A Review on Their Sampling and Extraction Techniques. *Molecules* **2022**, *27*, 3451. [CrossRef] [PubMed]
55. Malainey, M.E. The Reconstruction and Testing of Subsistence and Settlement Strategies for the Plains, Parkland, and Southern Boreal Forest. Ph.D. Thesis, University of Manitoba, Winnipeg, MB, Canada, 1997.
56. Eerkens, J.W. GC–MS analysis and fatty acid ratios of archaeological potsherds from the Western Great Basin of North America. *Archaeometry* **2005**, *47*, 83–102. [CrossRef]
57. Steiner-Bogdaszewska, Ż.; Tajchman, K.; Domaradzki, P.; Florek, M. Composition and fatty acid profile of bone marrow in farmed fallow deer (*Dama dama*) depending on diet. *Animals* **2022**, *12*, 941. [CrossRef] [PubMed]
58. Cordain, L.; Watkins, B.A.; Florant, G.L.; Kelher, M.; Rogers, L.; Li, Y. Fatty acid analysis of wild ruminant tissues: Evolutionary implications for reducing diet-related chronic disease. *Eur. J. Clin. Nutrition.* **2002**, *56*, 181–191. [CrossRef]
59. Schabereiter-Gurtner, C.; Saiz-Jimenez, C.; Piñar, G.; Lubitz, W.; Rölleke, S. Phylogenetic diversity of bacteria associated with Paleolithic paintings and surrounding rock walls in two Spanish caves (Llonín and La Garma). *FEMS Microbiol. Ecol.* **2004**, *47*, 235–247. [CrossRef]
60. Knief, C.; Altendorf, K.; Lipski, A. Linking autotrophic activity in environmental samples with specific bacterial taxa by detection of ^{13}C-labelled fatty acids. *Environ. Microbiol.* **2003**, *5*, 1155–1167. [CrossRef] [PubMed]